A Numerical Model of Coastal Upwelling[1]

JAMES J. O'BRIEN[2] AND H. E. HURLBURT[2]
National Center for Atmospheric Research[3], Boulder, Colo. 80302

(Manuscript received 17 September 1971)

ABSTRACT

A wind-driven model of coastal upwelling induced into a stratified, rotating ocean is solved numerically. The circulation is on an f plane and longshore variations are neglected. A multilevel model is derived, but only solutions for a two-layer model are discussed. A longshore baroclinic surface jet is discovered. The time-dependent geostrophic jet is dynamically explained by conservation of potential vorticity. The existence of the jet depends critically on stratification and non-zero wind stress at the coast. Coastal upwelling is confined to within 30 km of the shore. The model exhibits no deep countercurrent during active coastal upwelling. A time scale of the order of 10 days or longer is required for a pycnocline at 50 m depth to penetrate the surface. Solutions for a wide (>300 km) coastal shelf, an irregular shallow shelf, and a continental slope region are illustrated. A secondary upwelling region is found offshore at sharp breaks in the shelf topography. In all cases, the offshore flow is a simple Ekman drift and downwelling offshore is created by Ekman pumping caused by negative wind-stress curl.

1. Introduction

The phenomenon of oceanic upwelling off the west coasts of continents is important from physical and ecological viewpoints. The occurrence of strong upwelling of cold water in a narrow coastal strip contributes to increased productivity of the sea as well as to climate modification of the adjacent land. Smith (1968) has reviewed the physical process of upwelling. We will not review upwelling here, but we will cite various observational and theoretical papers as they are pertinent for support or comparison.

It is our intent to describe a simple theoretical model of the onset of upwelling by the use of numerical integration and scale analysis. We are interested in the physical description of the near-shore circulation induced into a stratified rotating ocean by the surface winds. A general multi-layer model is developed, but specific attention is confined to a two-layer ocean. The flow is on an f plane and longshore variations are neglected. The winds are steady but may vary offshore. The effects of wind-stress curl, bottom topography, and stratification are explored. Both barotropic and baroclinic modes are present in the model.

Following the derivation of the multi-layer model, we concentrate on describing a two-layer model of depth 200 m on a wide flat shelf. The numerical solution for an equatorward wind stress of 1 dyn cm^{-2} is presented to demonstrate the response of the system for this simplest case. Using the numerical solution as a guide for the scale analysis, we scale the model equations and the physics of the model are deduced. A time-dependent longshore jet is discovered. Finally, the two-layer model is solved for shelf configurations containing bottom topography.

2. Formulation of a general multi-layer model

Consider a stably stratified, rotating, incompressible fluid on a continental shelf-slope cross section near a north-south coast line. Suppose the fluid consists of m incompressible layers which have initial thickness $h_j(x)$ and densities ρ_j, $j=1(l)m$, counting down from the surface layer. We will assume in this model that north-south variations are neglected $(\partial/\partial y=0)$; the traditional Coriolis approximations apply; molecular transport of momentum is assumed to be unimportant compared to turbulent transport by eddy stresses; the fluid is hydrostatically balanced in the vertical; and the atmospheric pressure is uniform at the sea surface.

The appropriate coordinate system is a right-handed Cartesian coordinate system with x increasing eastward and z upward. The origin will be in the coastal cross section such that distances offshore are negative. In these initial studies, we shall neglect thermodynamic effects, i.e., the exchange of latent heat or sensible heat with the atmosphere is excluded as well as radiation. The latter may play an important role in the shallowest near-shore region. Also, no mixing of heat and salt between the ocean layers is considered. This is easily added if desired [see O'Brien (1967) for the details]. For upwelling induced by wind over several days, we are explicitly assuming that the time scale for vertical

[1] Contribution No. 55 of the Geophysical Fluid Dynamics Institute, Florida State University, Tallahassee.

[2] Permanent affiliation: Departments of Meteorology and Oceanography, Florida State University.

[3] The National Center for Atmospheric Research is sponsored by the National Science Foundation.

mixing is much slower than that for vertical transport of fluid.

We are particularly interested in the vertically averaged velocity within each layer and the vertical velocity at the interface of each layer. If the pertinent hydrodynamic equations of motion are integrated vertically over the depth of each layer and the vertically averaged horizontal velocity components u_j, v_j are assumed independent of depth within each layer, we obtain

$$\frac{\partial u_j}{\partial t}+u_j\frac{\partial u_j}{\partial x}+P_j=fv_j+[(\tau_j^{Tx}-\tau_j^{Bx})/\rho h_j]+A\frac{\partial^2 u_j}{\partial x^2}, \quad (1)$$

$$\frac{\partial v_j}{\partial t}+u_j\frac{\partial v_j}{\partial x}=-fu_j+[(\tau_j^{Ty}-\tau_j^{By})/\rho h_j]+A\frac{\partial^2 v_j}{\partial x^2}, \quad (2)$$

$$\frac{\partial h_j}{\partial t}+\frac{\partial h_j u_j}{\partial x}=0, \quad (3)$$

where P_j is the pressure integral for the layer and τ_j^T and τ_j^B are the stresses at the top and bottom of each layer. When $j=1$, $\tau_1^T=\tau_1^{Sx}+i\tau_1^{Sy}$, where these components are the wind stresses at the sea surface. They will be specified as functions of x and t. The vertical velocity is implicit in (3) and may be obtained *a posteriori* from the h_j and u_j fields. Both barotropic and baroclinic modes have been retained. The barotropic mode will be shown to be fundamentally important for the wind-driven upwelling problem. It has been neglected by previous investigators.

a. The pressure integrals

From the hydrostatic assumption, it follows that the pressure p_k at any point inside a layer k is given by

$$\left.\begin{aligned} p_1&=P_A+\rho_1 g\Big[\sum_{j=0}^{m-1}h_{m-j}+D(x)-z\Big], && \text{layer 1}\\ p_2&=P_A+\rho_1 g h_1+\rho_2 g\Big[\sum_{j=0}^{m-2}h_{m-j}+D(x)-z\Big], &&\\ &\vdots && \text{layer 2}\\ p_k&=P_A+\sum_{j=1}^{k-1}\rho_j g h_j+\rho_k g\Big[\sum_{j=0}^{m-k}h_{m-j}+D(x)-z\Big], && \\ & && \text{layer } k \end{aligned}\right\} \quad (4)$$

where m is the number of discrete layers, P_A the uniform atmospheric pressure, and $D(x)$ the elevation of the bottom above the reference level $z=0$. The influence of the torque of the atmospheric pressure gradient may be included if desired (e.g., Galt, 1971).

The x derivatives of these pressures are

$$\frac{\partial p_k}{\partial x}=\sum_{j=1}^{k-1}\rho_j g\frac{\partial h_j}{\partial x}+\rho_k g\left[\sum_{j=0}^{m-k}\frac{\partial h_{m-j}}{\partial x}+\frac{\partial D}{\partial x}\right]. \quad (5)$$

Integrating these over the appropriate layer, we find that

$$\begin{aligned} P_k h_k&=\frac{1}{\rho_k}\int_B^T\frac{\partial p_k}{\partial x}dz\\ &=\frac{h_k}{\rho_k}\sum_{j=1}^{k-1}\rho_j g\frac{\partial h_j}{\partial x}+h_k g\left[\sum_{j=0}^{m-k}\frac{\partial h_{m-j}}{\partial x}+\frac{\partial D}{\partial x}\right]. \end{aligned} \quad (6)$$

These values of P_k are used in (1). Thus, for an appropriate specification of the wind stress, a functional form of the interior stresses, and valid initial and boundary conditions, the formal statement of the problem will be complete.

The form of P_k can be simplified if either 1) the bottom layer (or layers) is at rest or 2) there is no bottom topography.

b. Initial conditions and boundary conditions

There are several allowable initial conditions. First, if the interface surfaces are horizontal, then the appropriate initial condition is $u_i=v_i=0$. If P_i does not vanish initially in any layer, the initial conditions may be $u_i=0$, $fv_i=P_i$, i.e., the layer is in geostrophic equilibrium.

The velocity components vanish at the coast, i.e., at $x=0$. At $x=-\infty$, the fluid velocity takes on its initial value. We anticipate specifying a wind-stress distribution that approaches zero far offshore. In such a case, a radiational condition (Shapiro and O'Brien, 1970) or a viscous far field (Galt, 1971) may be used to close the solution at a computational outer boundary. We will demonstrate that the solution in the upwelling zone is independent of the forcing outside the upwelling zone and thus apply far-field boundary conditions which cannot alter the solution near the coast in any significant way.

c. The interior stresses

The equations of motion (1)–(3) are coupled for adjacent layers through the pressure gradients P_j and the interior stresses. To complete the statement of the problem, we must specify a functional form of these stresses.

The stresses must be continuous across the interfaces, i.e., $\tau_j^{Bx}=\tau_{j+1}^{Tx}$ and $\tau_j^{By}=\tau_{j+1}^{Ty}$. They act in opposition to one another on the interface and thus are balanced. We wish to choose a functional form of $\boldsymbol{\tau}_j=\tau_j^x+i\tau_j^y$ dependent upon the velocity $\mathbf{q}_j=u_j+iv_j$, but not dependent upon $\partial\mathbf{q}/\partial z$. The logical physical choice is a quadratic form from a dimensional argument. To arrive at an appropriate form, let us consider the energy equation.

In general, for a continuously stratified system ($A=0$), one obtains an integral energy equation of the

form

$$\frac{\partial E}{\partial t}+\nabla_H\cdot\mathbf{J}=\int_B^T \mathbf{q}\cdot\frac{\partial\boldsymbol{\tau}}{\partial z}dz\equiv I, \tag{7}$$

where E is the sum of the kinetic and potential energy densities and $\mathbf{J}$ is an energy flux density. If we concentrate our attention on the integral on the right (I), we can arrive at an integrated expression for I and eventually at a form for $\boldsymbol{\tau}$. The approach outlined below was suggested by Robert O. Reid (personal communication) for a somewhat different problem.

Integrating I by parts, we obtain

$$I=[\mathbf{q}\cdot\boldsymbol{\tau}]_T-[\mathbf{q}\cdot\boldsymbol{\tau}]_B-\int_B^T \boldsymbol{\tau}\cdot\frac{\partial\mathbf{q}}{\partial z}dz. \tag{8}$$

If the velocity $\mathbf{q}$ or the stress $\boldsymbol{\tau}$ vanishes at the bottom, the second term vanishes. The first term is the rate of supply of kinetic energy from the winds. The integral on the right represents collectively the rate of decrease of energy of the organized motion, i.e., the rate of conversion to turbulence and ultimately to thermal energy. Moreover, from the second law of thermodynamics, we expect that the integrand

$$\boldsymbol{\tau}\cdot\frac{\partial\mathbf{q}}{\partial z}>0. \tag{9}$$

For a layered fluid system, this integral representing internal dissipation may be approximated by

$$I\equiv\int_B^T \boldsymbol{\tau}\cdot\frac{\partial\mathbf{q}}{\partial z}dz\approx\sum\boldsymbol{\tau}\cdot\Delta\mathbf{q}, \tag{10}$$

where the sum is taken over all internal surfaces.

Since I should be positive definite, a possible quadratic form for $\boldsymbol{\tau}$ is

$$\boldsymbol{\tau}_j^B=K_j\left[\frac{q_j+q_{j+1}}{2}\right](\mathbf{q}_j-\mathbf{q}_{j+1})=\boldsymbol{\tau}_{j+1}^T, \tag{11}$$

where $K_j>0$. An estimate of K_j can be obtained from observations of momentum exchange coefficients in the real ocean. O'Brien (1965) discussed the rationale necessary to estimate K_j. Note in (11) that q_j represents the magnitude of $\mathbf{q}_j$. It should be recognized that for a single layer the term $(\boldsymbol{\tau}_j^T-\boldsymbol{\tau}_j^B)$ represents both 1) the gain (loss) of kinetic energy from (to) the fluid layer above (below), and 2) the internal dissipation of kinetic energy through velocity shear of the mean velocity between the adjacent layers. In effect, we have specified a closure condition between the vertical mean structure in the fluid and the smaller scale turbulent motions.

3. The two-layer model

We will explore the details of a two-layer model. Consider a two-layer fluid governed by the dynamics derived in the previous section. The equations are

$$\frac{\partial u_1}{\partial t}+u_1\frac{\partial u_1}{\partial x}+g(h_1+h_2+D)_x=fv_1+(\tau^{Sx}-\tau^{Ix})/(\rho h_1)+A\frac{\partial^2 u_1}{\partial x^2}, \tag{12}$$

$$\frac{\partial v_1}{\partial t}+u_1\frac{\partial v_1}{\partial x}=-fu_1+(\tau^{Sy}-\tau^{Iy})/(\rho h_1)+A\frac{\partial^2 v_1}{\partial x^2}, \tag{13}$$

$$\frac{\partial h_1}{\partial t}+\frac{\partial h_1u_1}{\partial x}=0, \tag{14}$$

$$\frac{\partial u_2}{\partial t}+u_2\frac{\partial u_2}{\partial x}+g(h_1+h_2+D)_x-g'\frac{\partial h_1}{\partial x}=fv_2+(\tau^{Ix}-\tau^{Bx})/(\rho h_2)+A\frac{\partial^2 u_2}{\partial x^2}, \tag{15}$$

$$\frac{\partial v_2}{\partial t}+u_2\frac{\partial v_2}{\partial x}=-fu_2+(\tau^{Iy}-\tau^{By})/(\rho h_2)+A\frac{\partial^2 v_2}{\partial x^2}, \tag{16}$$

$$\frac{\partial h_2}{\partial t}+\frac{\partial h_2u_2}{\partial x}=0, \tag{17}$$

where

$$\left.\begin{aligned}\tau^{Ix}&=\rho c\bar{q}(u_1-u_2)\\ \tau^{Iy}&=\rho c\bar{q}(v_1-v_2)\\ \tau^{Bx}&=\rho cq_2u_2\\ \tau^{By}&=\rho cq_2v_2\\ q_i&=(u_i^2+v_i^2)^{\frac{1}{2}}\\ \bar{q}&=(q_1+q_2)/2\\ g'&=g(\rho_2-\rho_1)/\rho_2\end{aligned}\right\}. \tag{18}$$

The geometry is indicated in Fig. 1. The velocity components u_i, v_i are the instantaneous depth-averaged velocities for each layer. The subscript 1 refers to the upper layer and 2 to the lower layer. The layers are dynamically coupled through pressure gradient forces and interior stresses. It will be shown later that, for the chosen value of c, the interior stresses play no important role in the dynamics of the model.

It is possible to consider a variety of problems which can be solved using the basic model. We are particularly concerned here with the onset of upwelling. Assume that at $t=0$, h_1 and h_2+D are independent of x and $u_1=v_1=u_2=v_2=0$. We shall consider several different bottom topographies. As a standard case, consider a wide (>300 km) flat continental shelf of constant depth 200 m; let $h_1(x,0)=50$ m and $h_2(x,0)=150$ m. At $t=0$, an equatorward wind stress ($\tau^{Sy}=-1$) is impulsively applied. How does h_1 change as a function of space and time?

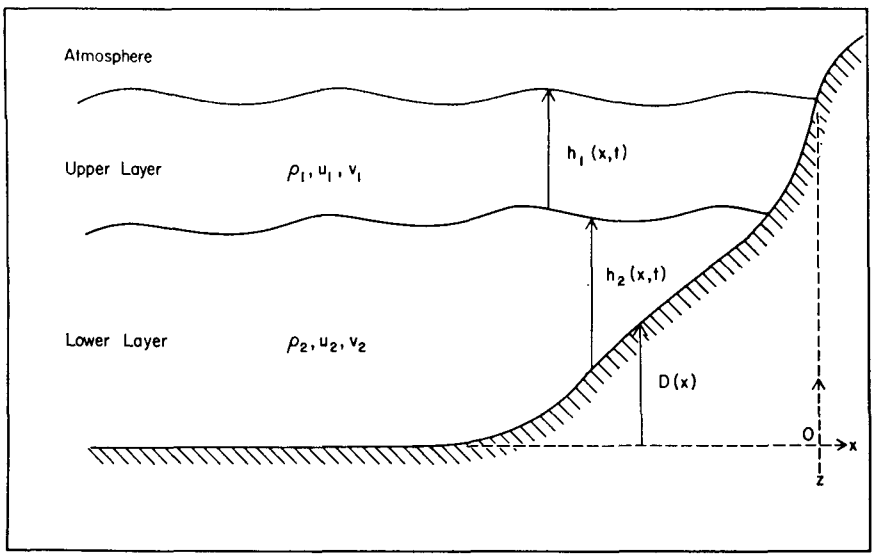

FIG. 1. Typical geometry for a two-layer model with a free surface and one interface. The bottom topography is $D(x)$, and h_1 and h_2 are the thicknesses of each layer of density ρ_1 and ρ_2. The velocities are depth-averaged.

For a nonlinear problem, we must resort to numerical methods of solution. The techniques used are new and extremely efficient, and they are explained in the next section.

Boundary conditions are required to close the problem. At the coast, $u_1=v_1=u_2=v_2=0$ and h_1 and h_2 are determined from the continuity equation using a one-sided finite difference. At $x=-\infty$, all of the velocities vanish and h_1 and h_2 are independent of time. In the computer model, we should utilize a radiational condition or the method of characteristics at some large but finite distance from the coast. However, empirical experimentation demonstrated that infinite channel (no slip) boundary conditions at a considerable distance (≥ 300 km) from the coast do not affect the solution in the coastal region.

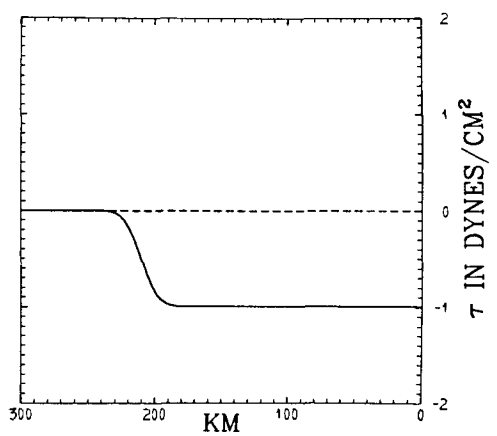

FIG. 2. Wind stress components as a function of distance offshore; τ^{Sy} is 1 dyn cm^{-2} near the coast; τ^{Sx} is zero everywhere.

It is practically impossible to obtain oceanographic estimates of $\tau(x,t)$ in upwelling regions. The data just do not exist. For this simple model, we choose a wind stress which is independent of time and space for $x\epsilon[0, -200$ km] and drops off rapidly in magnitude 200 km off the coast (Fig. 2).

The parameters for the standard case are $f=10^{-4}$ sec^{-1}, $g=10^3$ cm sec^{-2}, $D=0$, $\tau^{Sx}=0$, $\rho=1$, $A=10^6$ cm^2 sec^{-1}, $g'=2$, $c=3\times10^{-4}$. We have altered these for various computer solutions. The importance of the parameter values will become clearer in the section on scale analysis.

4. Semi-implicit method

We have designed an extremely efficient numerical scheme following the example of Kwizak and Robert (1971). For the present one-dimensional layered model, the scheme is sufficiently different from Kwizak and Robert that we shall present the technique in some detail.

Since the equations contain external gravity waves as solutions (as well as internal gravity waves), the garden variety explicit finite-difference schemes require a time step Δt bounded above by $\Delta x/(gH)^{\frac{1}{2}}$, where H is the total depth of the fluid. The fine resolution [$\Delta x=O(1$ km)] and the deep fluid [$H=O(1$ km)], envisioned for realistic simulation of coastal upwelling, dictate a time-step <1 min, whereas we anticipate integrating our model for days. Kwizak and Robert demonstrate that if we choose an implicit scheme for the terms which govern the physics of the fastest moving waves, a much larger time step may be utilized. We elect to treat both the external gravity wave and

the internal gravity wave modes implicitly. If the pressure gradient terms in the momentum equations and the divergence term in the continuity equations are treated implicitly, then we may use a much larger time step, say on the order of 1 hr. Application of the following scheme resulted in a factor of 20 savings in computer time for the present problem on a CDC 6600; i.e., a 20-min integration time using an explicit finite-difference scheme is reduced to less than 1 min by using the semi-implicit method. Identical results were obtained using both methods.

Consider the model equations in the form

$$\frac{\partial u_1}{\partial t}+g\frac{\partial}{\partial x}(h_1+h_2+D)=U_1, \tag{19}$$

$$\frac{\partial h_1}{\partial t}+H_1\frac{\partial u_1}{\partial x}=-h_1'\frac{\partial u_1}{\partial x}-u_1\frac{\partial h_1}{\partial x}\equiv D_1, \tag{20}$$

$$\frac{\partial u_2}{\partial t}+g\frac{\partial}{\partial x}(h_1+h_2+D)-g'\frac{\partial h_1}{\partial x}=U_2, \tag{21}$$

$$\frac{\partial h_2}{\partial t}+(H_2+D)\frac{\partial u_2}{\partial x}=-h_2'\frac{\partial u_2}{\partial x}-u_2\frac{\partial h_2}{\partial x}+D\frac{\partial u_2}{\partial x}\equiv D_2, \tag{22}$$

where H_1 is the mean depth of the upper layer and H_2+D the mean height of the interface between the two layers. No approximations have been made; U_1 and U_2 are all the remaining terms in the x-directed momentum equations. The linear part of the divergence term in the continuity equation is retained on the left-hand side. The primed quantities are defined by

$$\left.\begin{aligned}h_1&=h_1'+H_1\\ h_2&=h_2'+H_2\end{aligned}\right\}. \tag{23}$$

It is important to realize that H_1 and H_2+D are constants. We will treat the left-hand side of (19)–(22) implicitly and the right-hand side explicitly. (We have also made the horizontal diffusive terms implicit using the Crank-Nicholson method. This is not included below to simplify the discussion.) The tendencies are evaluated over $2\Delta t$ and the pressure gradient terms and the divergence terms are averaged between time levels $(n-1)\,\Delta t$ and $(n+1)\,\Delta t$.

The time-differenced equations are

$$u_{1j}{}^{n+1}+\left[\Delta tg\frac{\partial}{\partial x}(h_1+h_2+D)\right]_j^{n+1}$$
$$=2\Delta tU_{1j}{}^n+u_{1j}{}^{n-1}$$
$$-\left[\Delta tg\frac{\partial}{\partial x}(h_1+h_2+D)\right]_j^{n-1}\equiv L_1, \tag{24}$$

$$h_{1j}{}^{n+1}+\left[\Delta tH_1\frac{\partial u_1}{\partial x}\right]_j^{n+1}$$
$$=2\Delta tD_{1j}{}^n+h_{1j}{}^{n-1}-\left[\Delta tH_1\frac{\partial u_1}{\partial x}\right]_j^{n-1}\equiv L_2, \tag{25}$$

$$u_{2j}{}^{n+1}+\left[\Delta tg\frac{\partial}{\partial x}(h_1+h_2+D)-\Delta tg'\frac{\partial h_1}{\partial x}\right]_j^{n+1}$$
$$=2\Delta tU_{2j}{}^n+u_{2j}{}^{n-1}$$
$$-\left[\Delta tg\frac{\partial}{\partial x}(h_1+h_2+D)-\Delta tg'\frac{\partial h_1}{\partial x}\right]_j^{n-1}\equiv L_3, \tag{26}$$

$$h_{2j}{}^{n+1}+\left[\Delta t(H_2+D)\frac{\partial u_2}{\partial x}\right]_j^{n+1}$$
$$=2\Delta tD_{2j}{}^n+h_{2j}{}^{n-1}-\left[\Delta t(H_2+D)\frac{\partial u_2}{\partial x}\right]_j^{n-1}\equiv L_4. \tag{27}$$

All spatial derivatives are replaced by second-order finite differences. The subscripts j and n imply for any scalar q that

$$q_j{}^n=q(-j\Delta x,\ n\Delta t). \tag{28}$$

All of the right-hand side terms, defined now as L_i $(i=1,\ 2,\ 3,\ 4)$, are "known" at any time level in the calculations. We wish to find $(u_1,u_2,h_1,h_2)_j{}^{n+1}$ for all j at time level $(n+1)\,\Delta t$. Kwizak and Robert recommend elimination of the velocities and the solution of coupled Helmholtz equations for h_1 and h_2. Since we have homogeneous boundary conditions for u_1 and u_2, we elect to eliminate h_1 and h_2 from the above and obtain

$$u_{2j}{}^{n+1}-b\left[\frac{\partial^2 u_2}{\partial x^2}\right]_j^{n+1}+(c-a)\left[\frac{\partial^2 u_1}{\partial x^2}\right]_j^{n+1}=d, \tag{29}$$

$$-u_{1j}{}^{n+1}+u_{2j}{}^{n+1}+c\left[\frac{\partial^2 u_1}{\partial x^2}\right]_j^{n+1}=e, \tag{30}$$

where $a=gH_1\Delta t^2$, $b=g(H_2+D)\,\Delta t^2$, $c=g'H_1\Delta t^2$, and d and e are a linear combination of the L_i. These equations are coupled one-dimensional, Helmholtz equations in the unknowns $u_1{}^{n+1}$ and $u_2{}^{n+1}$ for all space points j. When the spatial derivatives are replaced by standard second-order finite differences, the resulting algebraic equations are tridiagonal and are easily solved by the special "up-down" variant of Gaussian elimination. In practice, we solve (29) and (30) iteratively by solving (30) for $u_{1j}{}^{n+1}$ using "up-down" and then (29) for $u_{2j}{}^{n+1}$. Only a few scans are needed for convergence.

The y-directed momentum equations are solved using well known techniques—leap-frog for time differences, a quadratic-averaging method known as Scheme F from Grammeltvedt (1969) for the advective terms, Crank-Nicholson for the diffusive terms, and centered-in-time

Coriolis terms. We believe it unnecessary to repeat these well-known finite-difference schemes here.

5. Flat shelf case

A simple flat shelf case is used to explore the basic physics of our model of the onset of upwelling. This standard model is integrated numerically until h_1 approaches zero near the wall. The solutions are shown in Figs. 3–10. The fluid is initially at rest with $h_1=50$ m, $h_2=150$ m for all x.

In Fig. 3, the height anomaly of the interface and free surface are shown after 4 days. Near the shore in a width of 20 km or so, the interface height anomaly is order 10 m. The free surface anomaly is order -20 cm. Offshore, where τ^S approaches zero, a negative height anomaly is calculated. We shall refer to positive height anomalies as upwelling and negative as downwelling. We shall demonstrate that the downwelling is simple Ekman pumping which occurs when curl τ^S is

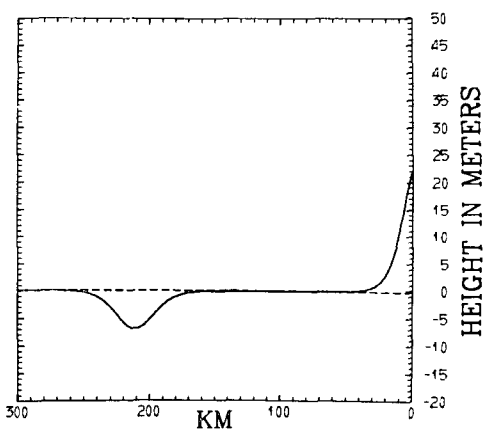

FIG. 3. Interface height anomaly after 4 days as a function of x. Upwelling is indicated by positive height anomaly near the shore. Downwelling is found centered at 210 km. The dashed line is the free surface anomaly.

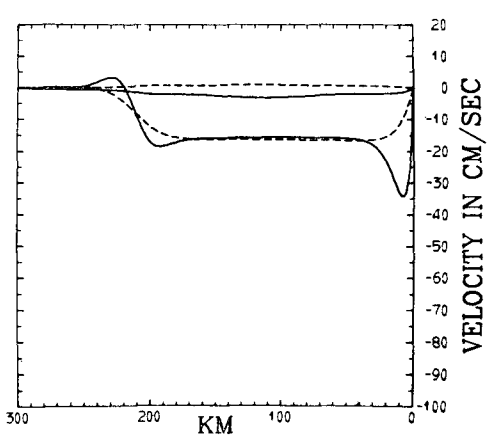

FIG. 4. Velocity profiles as a function of x after 4 days. The longshore flow v_1 exhibits a jet near 10 km offshore. The lower layer velocity profiles are dashed. The longshore velocities are barotropic between 50–150 km: $u_1<0$, $u_2>0$.

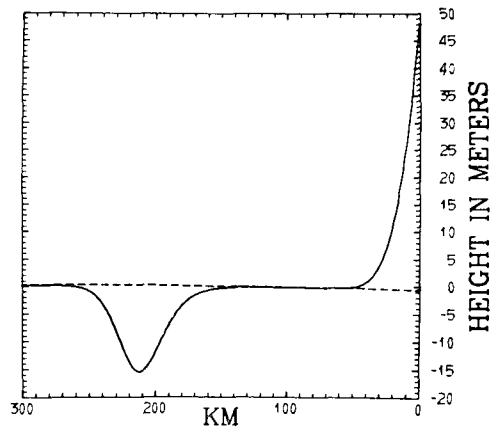

FIG. 5. Interface height anomaly after 10 days. The interface has almost surfaced near the shore. The downwelling is centered near 210 km. The dashed line is the free surface anomaly.

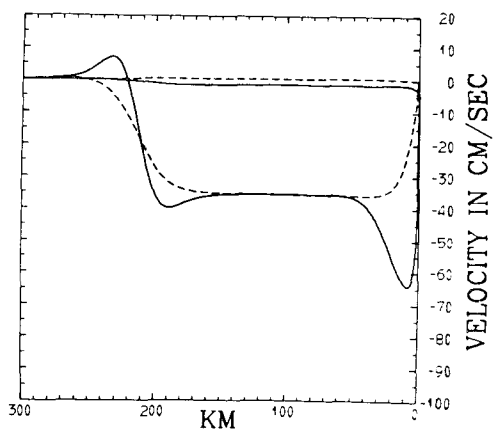

FIG. 6. Velocity profiles as a function of x after 10 days. Dashed lines are lower layer velocity components. A strong surface jet occurs near $x=0$. The longshore velocities are barotropic between 50–150 km.

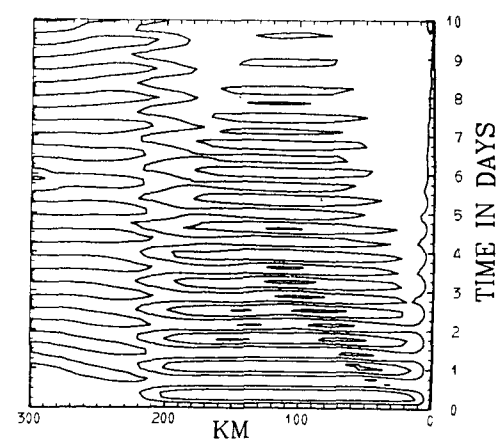

FIG. 7. Contours of u_1 as a function of time and space. The inertial oscillations are visible. The minimum u_1 is O(-3 cm sec^{-1}). The inertial oscillations decay in time in the forced region. The countour interval is 1 cm sec^{-1}.

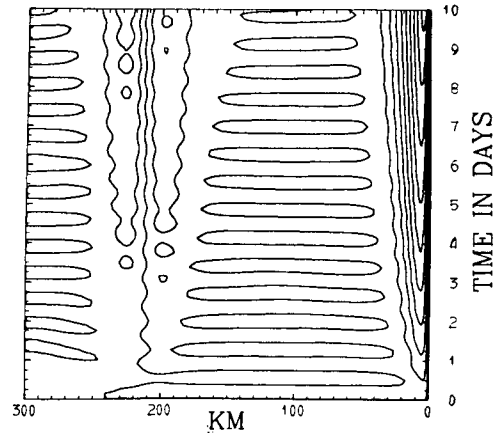

FIG. 8. Baroclinic velocity $v_1 - v_2$ contoured as a function of x and t. The heavy contour at $x=0$ indicates the presence of the jet. In the barotropic region, inertial oscillations of amplitude O(2 cm sec^{-1}) are found. The contour interval is 5 cm sec^{-1}.

negative. The dynamics of the upwelling at the wall are more complicated.

In Fig. 4, the four velocity components are shown after 4 days as a function of space. The upper layer flow is offshore ($u_1<0$); the lower layer is onshore ($u_2>0$) as expected with forcing by an equatorward wind stress in a rotating system. The longshore velocities are essentially southward everywhere. No substantial poleward flowing undercurrent is present. Near the coast, an equatorward flowing baroclinic jet is found in the upper layer. This is an important discovery. The dynamics of this jet will be discussed subsequently. The longshore flow is barotropic from 50–200 km. It will be shown to have dynamics similar to those of the coastal jet discussed by Charney (1955) in reference to the Gulf Stream and by Csanady (1968) relative to the coastal currents in a model Great Lake. Offshore, when τ^S approaches zero, the flow becomes baroclinic.

In Fig. 5, the interface height anomaly after 10 days is shown. The upwelling zone is order 30 km wide and

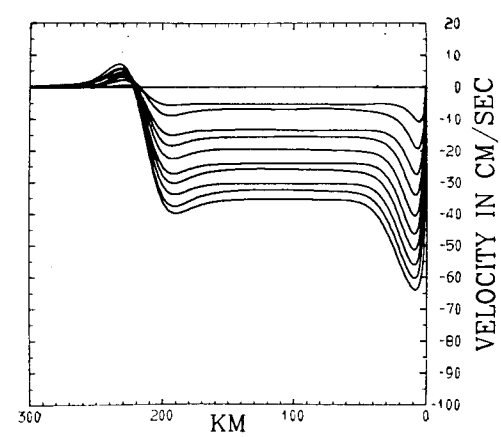

FIG. 9. Upper layer velocity v_1 as a function of x for each day. After 10 days, $v_1 = -64$ cm sec^{-1} in the jet. The uneven spacing of the lines is indicative of the inertial oscillation.

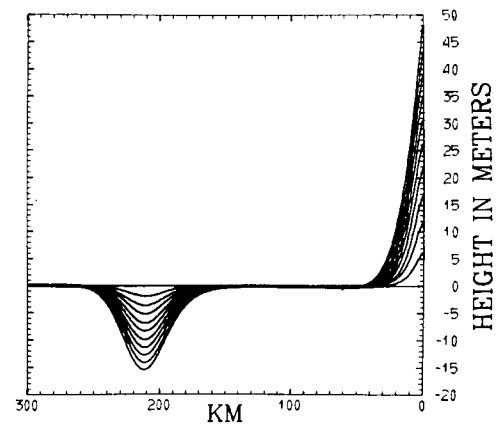

FIG. 10. Interface height anomaly for each day as a function of x. After 10 days, $h_1 = 2$ m at the wall and 65m near 210 km.

the height anomaly is almost 50 m, i.e., h_1 is approaching zero. The downwelling occurs 200 km offshore. The free surface anomaly is order -50 cm. It is important here to recognize that the upwelling occurs in a narrow (10–30 km) region against the coastal wall.

In Fig. 6, the velocities are shown after 10 days. The baroclinic jet, confined to the upper layer, is still the most striking feature. The longshore flow is barotropic from 50–150 km offshore. The baroclinic region at 200 km coincides with the region of non-zero wind-stress curl. Let us emphasize that the baroclinic region near 200 km may be shifted offshore as far as desired by appropriate redefinition of the wind-stress vector. In this paper, we are concerned only with the near-shore ocean circulation induced by steady winds. The influence of the large-scale ocean circulation dynamics is not considered.

In Fig. 6, the onshore flow in the lower layer is order 1 cm sec^{-1}. The offshore Ekman transport is order -2 cm sec^{-1}. As in the real ocean, the velocities exhibit strong inertial oscillations. In Fig. 7, an x, t plot of u_1 clearly shows the presence of the inertial oscillations. The inertial oscillations in the two layers are completely out of phase (Fig. 8). Schott (1971) has shown that inertial motions in an "almost two-layered" North Sea were highly coherent between the layers but 180° out of phase. The inertial oscillations in v_1 can be detected in Fig. 9 where v_1 is plotted for each day.

Fig. 10 illustrates the time evolution of h_1. The upwelling region is order 30 km wide near the coast.

Let us review the dynamics which lead to the developed flow seen in Figs. 3–10. At $t=0$, the equatorward stress drives an equatorward longshore velocity $v_1<0$. The Coriolis force rotates the flow 90° and offshore Ekman transport occurs, such that $u_1<0$. Due to the presence of the coast, a one-sided divergence occurs and h_1 decreases. Continuity requires compensating flow from below; thus, h_2 increases. Hence, we observe a shoreward transport $u_2>0$ in the lower layer. Far offshore where the wind-stress curl becomes nega-

tive, downwelling occurs through Ekman pumping. Except for the presence of the baroclinic jet and the narrowness of the upwelling region, this description is basically the classical Ekman (1905) physics. To explore the dynamics further, we find it instructive to non-dimensionalize the problem.

6. Non-dimensional two-layer model

On a coastal shelf, we expect *a priori* that there will be different velocity scales for u and v in each layer. Let primed quantities by non-dimensional; we define the scaling parameters.

$$\left.\begin{aligned}(u_i,v_i)&=(U_i,V_i)(u_i',v_i')\\ x&=Lx'\\ t&=Tt'\\ h_i&=H_ih_i'\\ (\tau^{Sx},\tau^{Sy})&=(\alpha\tau,\tau)(\tau^{Sx'},\tau^{Sy'})\\ (h_1+h_2+D)_x&=\frac{H}{L}(h_1'+h_2'+D')_x\end{aligned}\right\}. \tag{31}$$

We adopt the usual practice of dropping primes immediately.

Scaling the continuity equations implies that

$$U_2H_2=U_1H_1, \tag{32}$$

$$T=L/U_1, \tag{33}$$

where T is the time for the interface to surface. The former just demonstrates conservation of mass. We need to define several non-dimensional numbers:

$$\left.\begin{aligned}&R_i\equiv V_i/(fL)\ \text{[Rossby number]}\\ &F_i\equiv gH/(LfV_i)\\ &\quad\text{[Rossby number/external Froude number]}\\ &F_I\equiv g'H_1/(LfV_2)\\ &\quad\text{[Rossby number/internal Froude number]}\\ &E_H\equiv A/(\rho L^2f)\ \text{[a horizontal Ekman number]}\\ &E_D\equiv\tau/(\rho fU_1H_1)\ \text{[an Ekman drift]}\\ &A_i\equiv U_i/V_i\ \text{[velocity aspect ratios]}\end{aligned}\right\}. \tag{34}$$

The scaling is appropriate to the upwelling region next to the coast.

The scaled momentum equations for the two-layer model are

$$R_1A_1^2\left[\frac{\partial u_1}{\partial t}+u_1\frac{\partial u_1}{\partial x}\right]+F_1\frac{\partial}{\partial x}(h_1+h_2+D)$$
$$=v_1+\frac{\alpha\tau}{\rho H_1}\tau^{Sx}h_1^{-1}+E_HA_1\frac{\partial^2u_1}{\partial x^2}, \tag{35}$$

$$R_1\left[\frac{\partial v_1}{\partial t}+u_1\frac{\partial v_1}{\partial x}\right]=-u_1+E_D\tau^{Sy}h_1^{-1}+E_HA_1^{-1}\frac{\partial^2v_1}{\partial x^2}, \tag{36}$$

$$R_2A_2^2\left[\frac{H_2}{H_1}\frac{\partial u_2}{\partial t}+u_2\frac{\partial u_2}{\partial x}\right]+F_2\frac{\partial}{\partial x}(h_1+h_2+D)-F_I\frac{\partial h_1}{\partial x}$$
$$=v_2+E_HA_2\frac{\partial^2u_2}{\partial x^2}, \tag{37}$$

$$R_2\left[\frac{H_2}{H_1}\frac{\partial v_2}{\partial t}+u_2\frac{\partial v_2}{\partial x}\right]=-u_2+E_HA_2^{-1}\frac{\partial^2v_2}{\partial x^2}. \tag{38}$$

The interior and bottom stress terms are quite small, $O(10^{-2})$ or less, and the reader can easily demonstrate this after we deduce the size of the important scales in the problem. Thus, they do not appear above. We have demonstrated this numerically by calculating the magnitude of each term as a function of space and time.

We expect *a priori* that the velocity aspect ratios $A_i\ll1$ for each layer. The longshore flow will be directly coupled to the wind and is supported dynamically by the offshore pressure gradient. The numerical solutions tell us that L is order 10–30 km, which means that E_H is order 10^{-3}; this yields the geostrophic balance from (35) and (37)

$$F_1\frac{\partial}{\partial x}(h_1+h_2+D)=v_1, \tag{39}$$

$$F_2\frac{\partial}{\partial x}(h_1+h_2+D)-F_I\frac{\partial h_1}{\partial x}=v_2. \tag{40}$$

This implies $F_1=1$, $F_2-F_I=1$. If V_1 is 50 cm sec^{-1} and $L=30$ km, we obtain

$$\left.\begin{aligned}&H=15\text{ cm}\\ &V_2=17\text{ cm sec}^{-1}\text{ (near the shore)}\\ &V_2=V_1\text{ (away from the shore)}\end{aligned}\right\}. \tag{41}$$

The free surface depression near the coast is 15 cm and in the region of baroclinic flow $V_2<V_1$ as found numerically. Both longshore velocities are balanced geostrophically, but the baroclinic pressure gradient dramatically reduces the surface flow with depth. The jet must be confined to the surface layer.

Using the same scales, we find $R_1=1/6$ and $R_2=1/18$. As in most geophysical problems, the Rossby number is somewhat less than unity. If we accept that, away from the shore-bound upwelling region, τ^{Sy} must be balanced by the Ekman drift, then for this regime $E_D=1$, which implies $U_1=2$ cm sec^{-1} as found numerically. Near the shore, however, u_1 approaches zero and the balance must be

$$R_1\left[\frac{\partial v_1}{\partial t}+u_1\frac{\partial v_1}{\partial x}\right]=-u_1+E_D\tau^{Sy}h_1^{-1}+E_HA_1^{-1}\frac{\partial^2v_1}{\partial x^2}, \tag{42}$$

where $R_1\approx1/6$, $E_D=1$, $E_H\approx10^{-3}$, $A_1^{-1}\approx25$. This region should be rescaled and matched to the outer Ekman drift solution. But here we believe it sufficient to display

the multiple balance. The horizontal friction term is required to bring the longshore flow to zero at the wall. Therefore, on the shore side of the jet, v_{xx} will be important. The acceleration term must be important in the vicinity of the jet. In the steady state, there cannot be any jet. (This has been found numerically for large c, but not shown here.)

The presence of the jet depends on two important physical processes which are included in this model, but not in previous models of coastal upwelling. First, the wind stress may not vanish near the coast as in Hidaka (1954) and Hsueh and Kenney (1972). Secondly, the upwelling model must be truly time-dependent and not steady state as in Yoshida (1967) and Hidaka. Since the jet is observed in nature (Mooers, 1970; Mooers *et al.*, 1972), it is a real feature of coastal upwelling.

The scaling thus far has not clearly supported the dynamical basis for the jet; however, a potential vorticity argument does. Consider the equations

$$\frac{\partial v_1}{\partial t}+u_1\frac{\partial v_1}{\partial x}+fu_1=\frac{\tau^{sy}}{H_1\rho}, \tag{43}$$

$$\frac{\partial h_1}{\partial t}+\frac{\partial}{\partial x}(h_1u_1)=0, \tag{44}$$

$$\frac{\partial v_2}{\partial t}+u_2\frac{\partial v_2}{\partial x}+fu_2=0, \tag{45}$$

$$\frac{\partial h_2}{\partial t}+\frac{\partial}{\partial x}(h_2u_2)=0. \tag{46}$$

The potential vorticity equations are

$$\frac{d}{dt}\left(\frac{\frac{\partial v_1}{\partial x}+f}{h_1}\right)=0, \tag{47}$$

$$\frac{d}{dt}\left(\frac{\frac{\partial v_2}{\partial x}+f}{h_2}\right)=0, \tag{48}$$

where the curl of the wind stress near the coast has been neglected. Since the fluid is at rest initially, we may integrate once and obtain

$$\frac{\partial v_1}{\partial x}-f\left(\frac{h_1-h_{10}}{h_{10}}\right)=0, \tag{49}$$

$$\frac{\partial v_2}{\partial x}-f\left(\frac{h_2-h_{20}}{h_{20}}\right)=0, \tag{50}$$

where h_{10} and h_{20} are the initial profiles of h_1 and h_2. When upwelling occurs near the coast, $h_1/h_{10}<1$ and $h_2/h_{20}>1$. Therefore, v_1 must be a minimum at the coast and v_2 must be a maximum. This says that the jet and the upwelling region have the same width scale! Near the shore, the barotropic pressure gradient must increase since v_1 is geostrophic. This demonstrates the real importance of the free surface in the problem. When horizontal friction is included, the minimum in v_1 will be displaced away from the shore a distance

$$L_V=\left(\frac{AV_1}{fU_1}\right)^{\frac{1}{2}}\gtrsim 5 \text{ km}. \tag{51}$$

This estimate is obtained by setting $E_HA_1^{-1}=1$. Since A_1 decreases in the jet region, the estimate for L_V is a lower bound. This scaling predicts that the jet must vanish as we approach the equator. If A is large enough (10^8 cm^2 sec^{-1}) to permit the viscous boundary layer to envelop the entire upwelling region, no jet will develop. These conclusions have been verified numerically. It is our thesis that horizontal eddy viscosity must not be allowed to play a dominant role in more complicated models of coastal upwelling, since real physical features of the circulation will be smeared away.

For the v_2 momentum equation, the outer balance is

$$R_2\frac{H_2}{H_1}\frac{\partial v_2}{\partial t}=-u_2. \tag{52}$$

The onshore flow is balanced by the tendency term when $H_2>H_1$. Since the Ekman drift offshore will always be confined to a thin upper layer even in a continuously stratified ocean, this balance must be valid. The absence of the longshore pressure gradient to balance u_2 confuses our physical argument. Garvine (1971) allows a constant (but small) longshore pressure gradient for his steady-state model. However, a consequence of his model is that the vertical integral of the longshore flow must vanish. This is rarely observed. He does obtain a deep poleward flowing countercurrent which does not appear in our model. From our model, we conclude that the commonly observed deep countercurrent is produced by the large-scale circulation (Pedlosky, 1969; Durance and Johnson, 1970) and not by the local wind-induced upwelling. This is, of course, sheer speculation which must be tested in fully three-dimensional models of coastal upwelling.

Near the shore, i.e., where ($|x|<5$ km), v_{2xx} must increase to bring v_2 to zero at the wall, as for the upper layer. There are two balances for the lower layer y-directed momentum equation: an outer inertial solution and an inner solution dominated by friction.

In summary, the longshore velocities v_1, v_2 are balanced geostrophically by a 15-cm surface slope in 30 km. The baroclinic pressure gradient reduces the flow in the lower layer. The offshore Ekman drift is 2 cm sec^{-1}. The tendency terms for v_1, v_2 are important

TABLE 1. Values of parameters and scaling variables.

U_1	2 cm sec^{-1}	f	10^{-4} sec^{-1}
U_2	$\frac{2}{3}$ cm sec^{-1}	g	10^3 cm sec^{-2}
V_1	50 cm sec^{-1}	g'	2 cm sec^{-2}
V_2	17 cm sec^{-1}	A	10^6 cm^2 sec^{-1}
H_1	5×10^3 cm	τ	1 dyn cm^{-2}
H_2	15×10^3 cm	ρ	1 gm cm^{-3}
H	15 cm	c	3×10^{-4}
L	30 km	Δx	1 km
T	10 days	Δt	30 min
		α	10^{-1}

in the dynamics of the model. The time scale $T=L/U_1$ is order 10 days or larger. This means that the interface, originally at 50 m, will surface in about 10 days. This implies an average vertical velocity of 3×10^{-3} cm sec^{-1}. In the real ocean, the decrease of temperature with depth will allow appearance of cold upwelled water almost immediately after the onset of upwelling. However, our solution implies that it will take several days for a subsurface thermocline or pycnocline to appear at the surface as an oceanic front.

The assumed values of the parameters and the deduced values of the scaling variables are given for convenience in Table 1. The reader should realize that if a larger value of the bottom drag coefficient c is used, bottom friction will be important in the v_2 momentum equation. We have tried to reduce the dynamic role of bottom friction in our upwelling model by keeping c small. The kinematic role of bottom friction has been retained. In the numerical solutions given in this paper, the interface surfaces (and the computations are terminated) before bottom or internal stresses play any appreciable role in the dynamics of the problem.

The downwelling occurs through Ekman pumping. Far offshore, the balance in (36) can only be

$$u_1h_1=\tau^{Sy}, \tag{53}$$

whose curl is

$$\frac{\partial u_1h_1}{\partial x}=\frac{\partial \tau^{Sy}}{\partial x}=-\frac{\partial h_1}{\partial t}. \tag{54}$$

Since curl $\tau<0$ offshore, h_1 must increase; thus, downwelling is simulated. If τ varies in x, the downwelling will be distributed offshore according to (54). In our model, the upwelling at the coast is driven by a narrow band of wind stress of east-west extent greater than 30 km, but the downwelling occurs due to the wind-stress curl.

7. Sharp-shelf case

The second numerical solution to be discussed is a fictitious sharp-shelf case (Fig. 11). Suppose that the 200 m depth continental shelf is wide (>300 km), but shoreward of 100 km there exists a shallow inshore shelf of depth 64 m. We assume that the undisturbed pycnocline is at 50 m. Over the shallow shelf, the lower layer is only 14 m thick, whereas seaward of 100 km it is 150 m thick. The wind stress profile is identical to the standard case (Fig. 2).

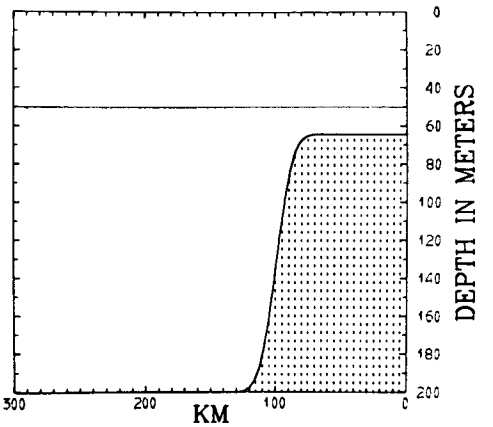

FIG. 11. Geometry for the sharp-shelf case. The upper layer is 50 m thick initially. The lower layer is 14 m thick near the coast and 150 m thick offshore.

The numerical solutions are shown in Figs. 12–16. In Fig. 12, the velocity profiles after 10 days' integration are shown. The effect of the shelf is clearly seen. The upper layer flow offshore (u_1) is unchanged. The compensating onshore flow in the lower layer increases as the sea bottom rises near 100 km. The longshore velocities are barotropic between 50–150 km. A weak nearshore jet in v_1 is still evident. At 210 km, the wind stress curl creates a secondary baroclinic region. In Fig. 13, the height anomaly for the upper layer is shown as a function of time. A weak secondary upwelling region is found at 100 km. The potential vorticity argument, (49), easily explains the dynamics of the secondary upwelling region. After a few days, this actually decreases, but at the shore the upwelling is still occurring. Comparing Figs. 10 and 13, we observe that the presence of the bottom topography

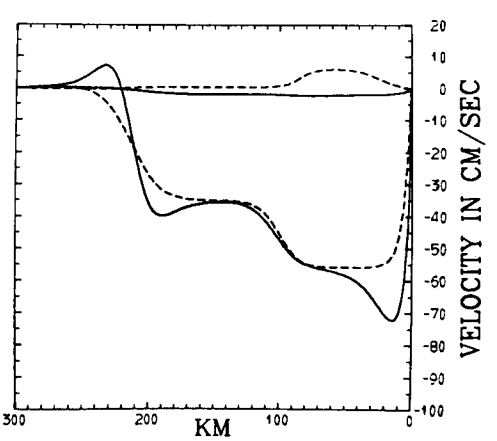

FIG. 12. Velocity profiles after 10 days for the sharp-self case. The lower layer velocity profiles are dashed. The longshore flow exhibits a slight jet in the upper layer and is essentially barotropic from 50–150 km.

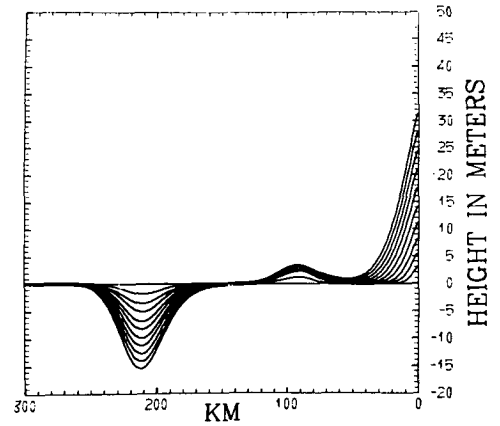

FIG. 13. Interface height anomaly profiles for each day. After 10 days, $h_1 = 19$ m at the coast.

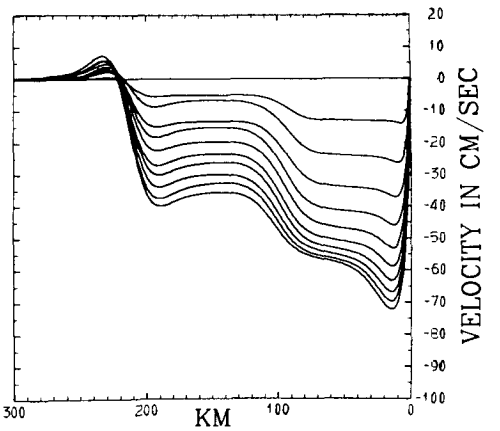

FIG. 14. Profiles of v_1 each day for the sharp-shelf case. The uneven spacing of the lines indicates the inertial oscillations.

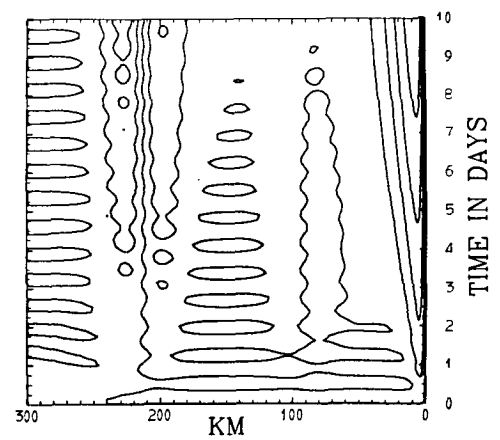

FIG. 15. Contours of $v_1 - v_2$ as a function of time and space for the sharp-shelf case. The contour interval is 5 cm sec^{-1}. The amplitude of the inertial oscillation at 150 km is O(2 cm sec^{-1}). The solid line at the coast indicates the baroclinic jet.

delays the upwelling at the coast. In the standard case, $h_1 = 2$ m after 10 days, but $h_1 = 19$ m in the sharp-shelf case after 10 days. The downwelling in this case also

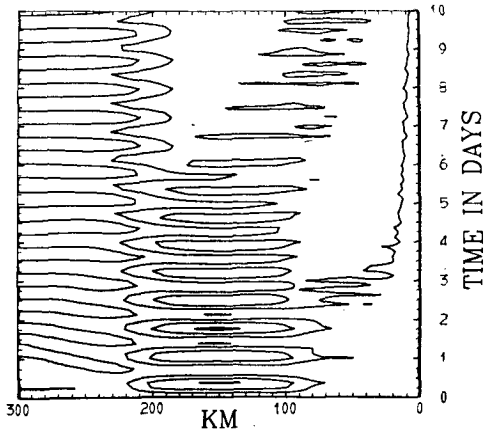

FIG. 16. Contours of u_1 as a function of time and space for the sharp-shelf case. The contour interval is 1 cm sec^{-1}. The inertial oscillations near 150 km have an amplitude of 2 cm sec^{-1}.

occurs offshore at 210 km in response to the negative wind stress curl.

The evolution of v_1 is shown in Fig. 14. The uneven spacing of the lines indicates the presence of the inertial oscillations. These are seen more clearly in Fig. 15 where the baroclinic velocity $v_1 - v_2$ is contoured as a function of time. It is of interest to observe that the amplitude of the inertial oscillation is damped over the shelf. In Fig. 16, u_1 is contoured on the x, t plane. The strong inertial oscillations are primarily observed between 100–200 km. At 6 days (when the secondary upwelling has diminished at the edge of the shelf), the pattern of the inertial oscillations is affected by a shoreward propagating internal wave.

8. Oregon coast case

There is some value in integrating a case with bottom topography similar to the Newport, Oregon region, since considerable amounts of direct current observations have been acquired in this area by Oregon State University. In Fig. 17, the simulated topography

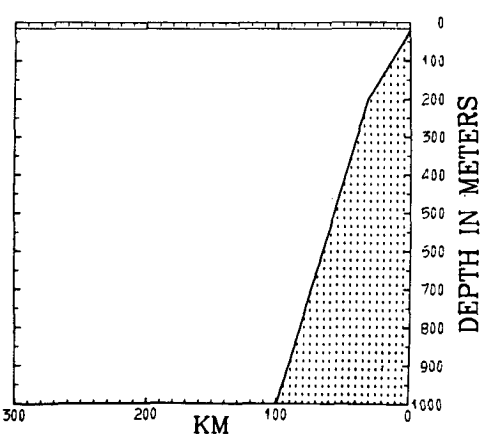

FIG. 17. Bottom topography for the simulated Oregon Coast case. The upper layer is 15 m thick initially. The lower layer is 1 km thick offshore.

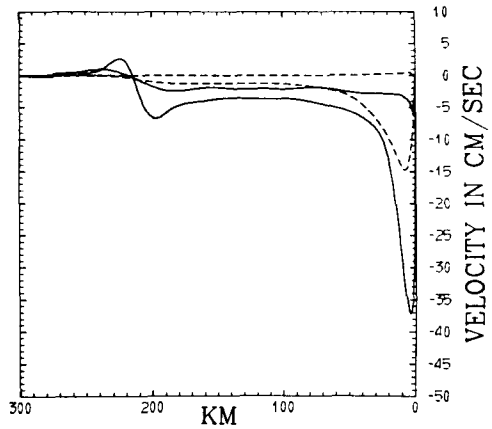

FIG. 18. Velocity profiles after 3 days for the Oregon Coast case. The lower layer velocity profiles are dashed. A narrow jet in v_1 is centered at 5 km offshore.

for this case is shown. The shelf drops off to 200 m by 30 km offshore and to 1 km depth at 100 km offshore. In this example, we choose the upper layer to be only 15 m thick. This is necessary to avoid a major reprogramming effort. Sielecki and Wurtele (1970) have shown how to integrate the shallow water equations in a basin with sloping sides. Their ideas are being left for future work.

We adopt the same wind stress profile (Fig. 2) with 0.5 amplitude in τ^{Sy}. The velocity profiles after 3 days are shown in Fig. 18. The longshore jet is narrow, O(15 km). The solution is essentially barotropic from 50–150 km. In Fig. 19, the height anomaly is shown as a function of time. Since the upper layer is quite thin (15 m) initially, the interface has almost surfaced in 3 days. The downwelling occurs, as predicted, at 210 km offshore.

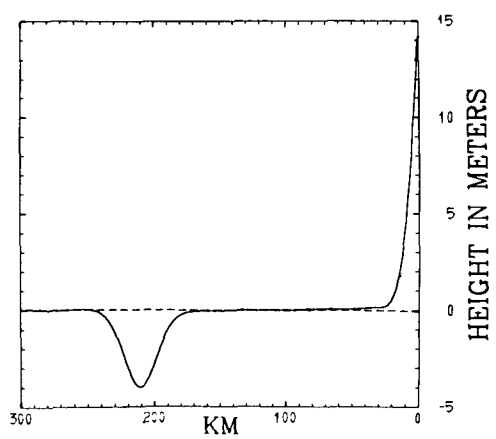

FIG. 19. Interface height anomaly for the Oregon Coast case after 3 days. The interface has risen at the coast to within 1 m of the surface. Downwelling occurs offshore at 210 km.

9. Critique

We have idealized coastal upwelling in this paper. Even within the framework of our layered model, it is possible to vary many parameters. We have run numerous solutions, O(100), varying bottom topography, wind stress, stratification, latitude, frictional constants, etc. Space does not permit a full disclosure of these results. There are some comments, however, that are appropriate.

Our simple two-layer model has no realistic steady-state solution. Examination of (14) and (17) will convince the reader that the only steady-state solution is $u_1=u_2=0$ everywhere. The longshore velocities are geostrophic and the three y-directed vertical and horizontal stresses must balance. Clearly, the role of the north-south pressure gradient must be included to balance non-zero x-directed motion in a realistic steady state. Since steady-state motion never occurs in the real ocean and we are concerned with the onset of upwelling over a few days, we do not regard this as a serious problem. It is our intention to develop fully three-dimensional models in the future.

In real eastern boundary currents, a deep poleward flowing countercurrent is almost always present (Wooster and Reid, 1963). Our model has no mechanism for producing a countercurrent. Huyer (1971) has shown that during a period of strong upwelling off the Oregon Coast the countercurrent is greatly diminished.

Hidaka (1954) reported that upwelling is a maximum, when the wind is equatorward but with an angle 21° offshore. We do not concur. In our stratified model, the maximum rate of upwelling occurs when the wind is only slightly offshore [O(5°)]. As f decreases and we approach the equator, this angle increases; at 4N the angle is O(30°) (solutions not shown). The wind angle for maximum upwelling is an unknown function of latitude, stratification, depth of the upper mixed layer, and time.

10. Summary

A two-layer numerical model of coastal upwelling in a stratified ocean on an f plane has been solved. A geostrophic baroclinic surface jet has been discovered and explained dynamically by a potential vorticity argument. The coastal upwelling and the jet are shown to be confined to within 30 km of the coast.

Considerable experimentation can be done with the model described here. We have performed many numerical experiments varying the parameters of the model. Solutions with several layers and time-dependent winds have been obtained, but these must be reported elsewhere. It seems essential that the next generation of numerical models of coastal upwelling must be three-dimensional to explore the dynamic role of the north-south pressure gradient and the north-south divergence.

Acknowledgments. This paper is the basis of a master's thesis for Mr. Hurlburt in the Department of Meteorology, Florida State University. Mr. Hurlburt has been partially supported by a NASA fellowship. J. J. O'Brien has been supported by NCAR during the summers of 1970 and 1971. The Computer Facility at NCAR has provided CDC 6600 time for the computations. The Florida State University Computing Center has provided some computer time on its CDC 6400. The bulk of the research costs was supplied by the Office of Naval Research under Contract NONR-N00014-67-A-235-0002 at Florida State. Partial support has been derived from National Science Foundation under Grant GA-29734.

We wish to acknowledge the encouragement, insight and support of Phil Hsueh, Christopher Mooers, John Allen, Dana Thompson and Richard McNider during the evolution of this research.

REFERENCES

Cherney, J. G., 1955: The generation of oceanic currents by wind. *J. Marine Res.*, **14**, 477–498.

Csanady, G. T., 1968: Motions in a model Great Lake due to a suddenly imposed wind. *J. Geophys. Res.*, **73**, 6435–6447.

Durance, J. A., and J. A. Johnson, 1970: East coast ocean currents. *J. Fluid Mech.*, **44**, 161–172.

Ekman, V. W., 1905: On the influence of the earth's rotation on ocean currents. *Arkiv. Mat. Astron. Fysik.*, **12**, 1–52.

Galt, J. A., 1971: A numerical investigation of pressure-induced storm surges over the continental shelf. *J. Phys. Oceanogr.*, **1**, 82–91.

Garvine, R. W., 1971: A simple model of coastal upwelling dynamics. *J. Phys. Oceanogr.*, 1, 169–179.

Grammeltvedt, A., 1969: A survey of finite-difference schemes for the primitive equations for a barotropic fluid. *Mon. Wea. Rev.*, **97**, 384–404.

Hidaka, K., 1954: A contribution to the theory of upwelling and coastal currents. *Trans. Amer. Geophys. Union*, **35**, 431–444.

Hsueh, Y., and R. N. Kenney III, 1972: Steady coastal upwelling in a continuously stratified ocean. *J. Phys. Oceanogr.*, **2**, 27–33.

Huyer, A., 1971: A study of the relationship between local winds and currents over the continental shelf off Oregon. M. S. thesis, Oregon State University, Corvallis.

Kwizak, M., and A. Robert, 1971: A semi-implicit scheme for grid point atmospheric models of the primitive equations. *Mon. Wea. Rev.*, **99**, 32–36.

Mooers, C. N. K., 1970: The interaction of an internal tide with the frontal zone in a coastal upwelling region. Ph.D. dissertation, Oregon State University, Corvallis.

——, R. L. Smith, C. A. Collins and J. G. Pattullo, 1972: The dynamic structure of the frontal zone in the coastal upwelling region off Oregon. *Deep-Sea Res.* (in press).

O'Brien, J. J., 1965: The non-linear response of a two-layer, baroclinic ocean to a stationary, axially-symmetric hurricane. Tech. Rept., Ref. 65-34T, Texas A & M University, 99 pp.

——, 1967: The non-linear response of a two-layer, baroclinic ocean to a stationary, axially-symmetric hurricane: Part II. Upwelling and mixing induced by momentum transfer. *J. Atmos. Sci.*, **24**, 208–215.

Pedlosky, J., 1969: Linear theory of the circulation of a stratified ocean. *J. Fluid Mech.*, **35**, 185–205.

Schott, F., 1971: Spatial structure of inertial-period motions in a two-layered sea, based on observations. *J. Marine Res.*, **29**, 85–102.

Shapiro, M. A., and J. J. O'Brien, 1970: Boundary conditions for fine-mesh forecasting. *J. Appl. Meteor.*, **9**, 343–349.

Sielecki, A., and M. G. Wurtele, 1970: The numerical integration of the nonlinear shallow-water equations with sloping boundaries. *J. Comput. Phys.*, **6**, 219–236.

Smith, R. L., 1968: Upwelling. *Oceanographic Marine Biology, Annal Review*, Vol. 6. London, Geo. Allen and Unwin, Ltd., 11–47.

Wooster, W. S., and J. L. Reid, Jr., 1963: Eastern boundary currents. *The Sea*, Vol. 2, New York, Interscience, 253–280.

Yoshida, K., 1967: Circulation in the eastern tropical oceans with special reference to upwelling and undercurrents. *Japan. J. Geophys.*, **4**, No. 2, 1–75.